Rock fabric, petrography, mineralogy, log analysis and core analysis of the Palaeocene Mey sandstone reservoir planned for CCS

Y. BEKBEROV

School of Environmental Sciences, University of Liverpool, Jane Herdman Building, 4 Brownlow Street, Liverpool, United Kingdom, L69 3GP

psybekbe@liv.ac.uk

Supervisors: Prof R H Worden and Dr M Allen

Abstract: One of Carbon Capture and Storage (CCS) subsurface reservoirs that have been proposed as a CO_2 storage site is the Palaeocene turbidite Mey Sandstone Member, Outer Moray Firth, UKCS. The aim of the project is to integrate the core sedimentology with core analysis, chemostratigraphy and mineralogy data, to fundamentally reveal what controls the porosity and the permeability, and so better understand how to model the sandstone for future CO_2 injection. From the seismic or even wireline data, sections of these types of sandstone tend to be interpreted as homogeneous section of sand ("tanks of sand"). However, the analysis of XRF (X-ray Fluorescence) and LPSA (Laser particle size analysis) data revealed that there are distinct stratigraphic variations that relate to some subtle variations in porosity and permeability. Core description identifies the two main packages of sandstone within this well. Chemical composition reveals that clay content is a significant control and affects the sorting of the Mey sandstone, that is, in turn, affects the reservoir quality. The top section is characterized by better reservoir quality, sorting, less clay content and interbedded with the claystone clasts. Bottom section with continuous vertical stratigraphy has the poorer sorting, more clay content, calcite cemented intervals and uncommon high pyrite minerals.

CO_2 is one of the compounds that affect the climate on Earth. Recent agreements urged the scientific society to propose new methods to reduce the emission of CO_2 into the atmosphere to combat the rise of temperature (ZEP 2015). The development of a carbon dioxide capture and storage (CCS) was proposed as one of the main techniques in this case. The aim of the CCS is the capture the CO_2 from fossil-fired power station and other industrial factories and to transport it in the subsurface reservoirs (such as depleted hydrocarbon reservoirs, unminable coal-seams and saline aquifers) to store in safe manner (Haszeldine *et al*. 2018; Flude *et al.* 2018). The subsurface reservoir should have the needful reservoir quality to properly store the CO_2 such as the porosity to bear the substance in pore spaces, the permeability to make sure that it is going to flow while injecting, having a proper caprock to prevent CO_2 from the leakage, the trapping architecture and laterally and vertically extensive homogeneous rock to secure it in the desired volume. So, it is pretty similar to conventional reservoir plays.

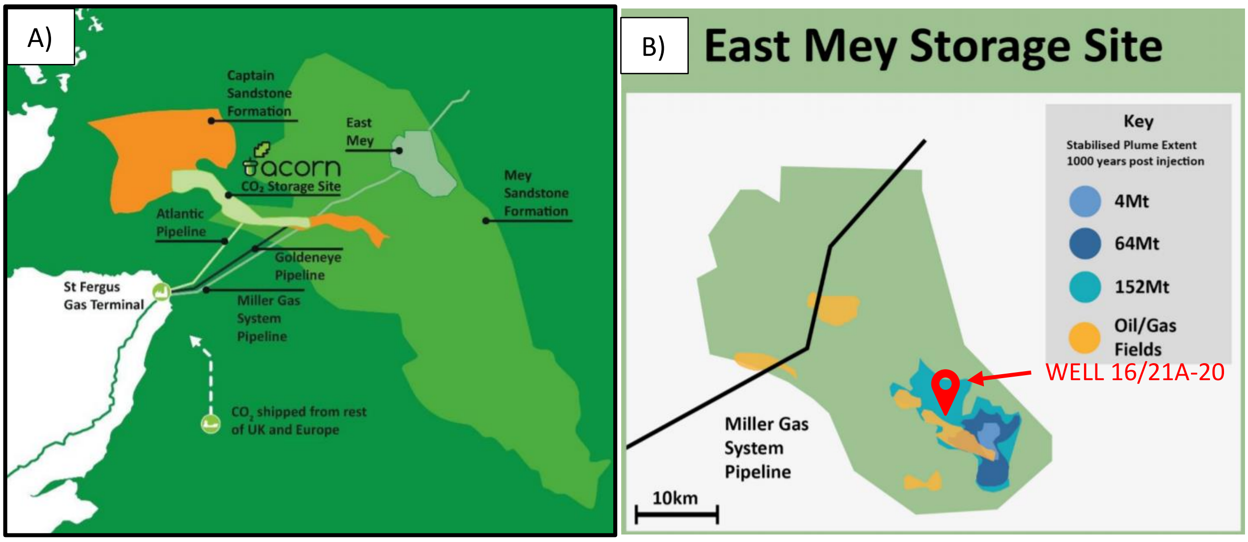

Figure 1. *A) Map of the Acorn CO_2 storage site project infrastructure showing two storage site units: Captain sandstone formation and Mey sandstone formation. B) Map of the East Mey storage site plan where the location of the well is pointed (adapted from Lynch 2019).*

The East Mey storage site was proposed as one of the CO_2 storage sites in the UK due to close location to the developed oil industry infrastructure and pipelines (Lynch 2019). The Paleocene Mey sandstone is the main rock of this storage site and was proven as the oil-bearing reservoir with the needed quality. This sandstone classified as the turbidite type deep-marine sandstone because it was deposited by turbidity and gravitation flow from the shelf to the basin through the slope. Due to multiple source entry points it is laterally extensive and relatively massive sheet-like sand body (Kilhams *et al.* 2012).

The mentioned East Mey storage site is located in the Outer Moray firth basin close to the border between the UK and Norway. Several wells were drilled in this area and some of them detected small oil fields. One of the exploration wells is [24] 16 21a-20 is the source of the information about the Mey sandstone and located in the middle of the East Mey storage site. It was drilled by Sun Oil Britain Ltd in 1990 as a deviated appraisal well. Core sections were taken as well as coring and core analysis (CCA) and wireline logs during the exploration (Sun Oil Britain Ltd. 1990). Two core sections were derived from the Mey (Andrew) sandstone formation. The well was then suspended for several decades, and new interest for the data taken was caused recently by the CCS study of the Mey sandstone. Quantitative Evaluation of Minerals by Scanning (QEMSCAN) and X-Ray diffraction (XRD) was made to further understand the rock for the CCS study.

The purpose for coring the sections in the Mey sandstone was to detect the oil-water contact as from the resistivity logs the sandstone in this interval showed the high value (Sun Oil Britain Ltd. 1990). A new perspective of the Mey sandstone is to prove that this reservoir can be suitable to inject CO_2. As it can be seen from the data taken, the Mey sandstone is homogeneous rock with relatively high porosity/permeability, having a good response from the resistivity and gamma log. Deposition of the Mey sandstone was by the process of turbidity current and gravity flow and it was interrupted by the deep-sea sedimentation of the fine-grain material of the Lista formation that is observed as mudstones and can play the positive role of the caprock and the negative role as the flow barrier because the cyclicity of turbidite sedimentation results in suspension of the turbidites. It can cause the chemical composition change of the reservoir rock itself due to diagenesis and therefore, change in the composition of the reservoir rock. Other diagenetic change can cause the compaction and carbonate cementation because depositional area was in the marine settings. Thereby, the variation in composition within the rock should be better studied. From the point of CCS, injection of any substance in the subsurface is highly sensible process, even more if it is the highly reactive CO_2 and study of the reservoir rock, as it is the main control, should be by assessing any possible risks. As a result, the new study of rock fabrics, mineralogy and petrography of the Mey sandstone in terms of the characterisation its homogeneity of the rock is became required. To define the main research interest of the rock, the following questions of the study are listed:

1. What is the relationship between CCA and QEMSCAN derived porosity/permeability and the stratigraphy (facies, top and bottom interval)?
2. What is the variation in terms of grain size/sorting within the cored section/stratigraphy and how it controls the porosity and permeability?
3. What is the variation of the rock composition within the cored section/stratigraphy and how it controls the porosity, permeability and possibly the grain size/sorting?

Geological background

The North Sea is one of the well-studied regions of the geological interest (Glennie 2009). Deep-sea turbidite siliciclastic sediments were deposited in the Paleocene and Eocene periods and have been proved as the reservoir for hosting hydrocarbons. In the UK part of the North Sea these turbidites were deposited in the Outer Moray firth and in a direction of the Viking graben in the Central North Sea.

Deegan and Scull (1977) proposed the lithostratigraphic scheme for the Central North Sea and it has two subdivisions: The Moray and the Montrose groups. The Mey sandstone member, that is the studied rock formation, relate to the Montrose group of the Paleocene age.

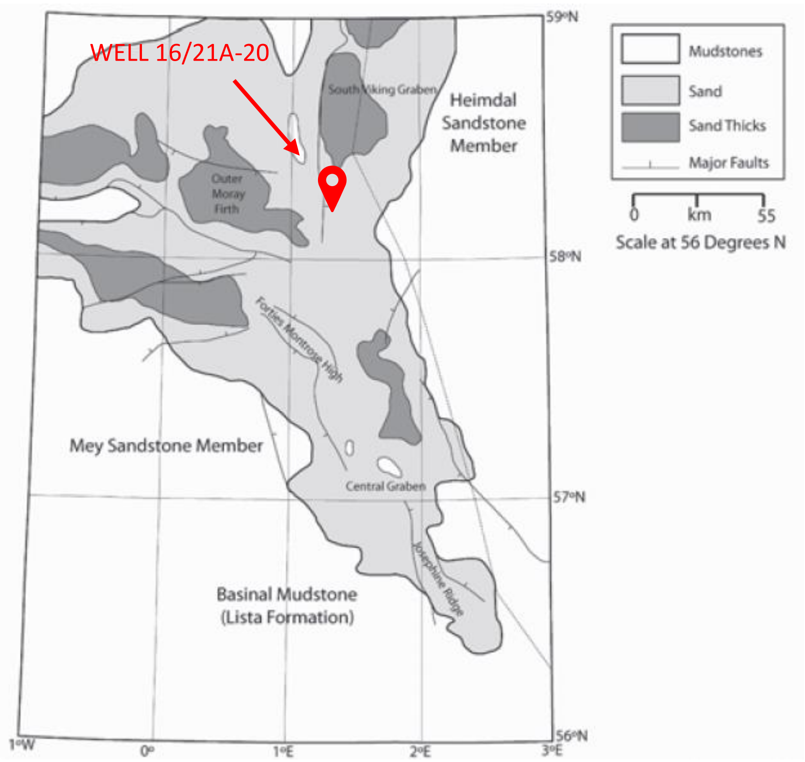

Figure 2. *Facies distribution of the Mey sandstone member and the well location (adapted from Mudge and Bujak 1996)*

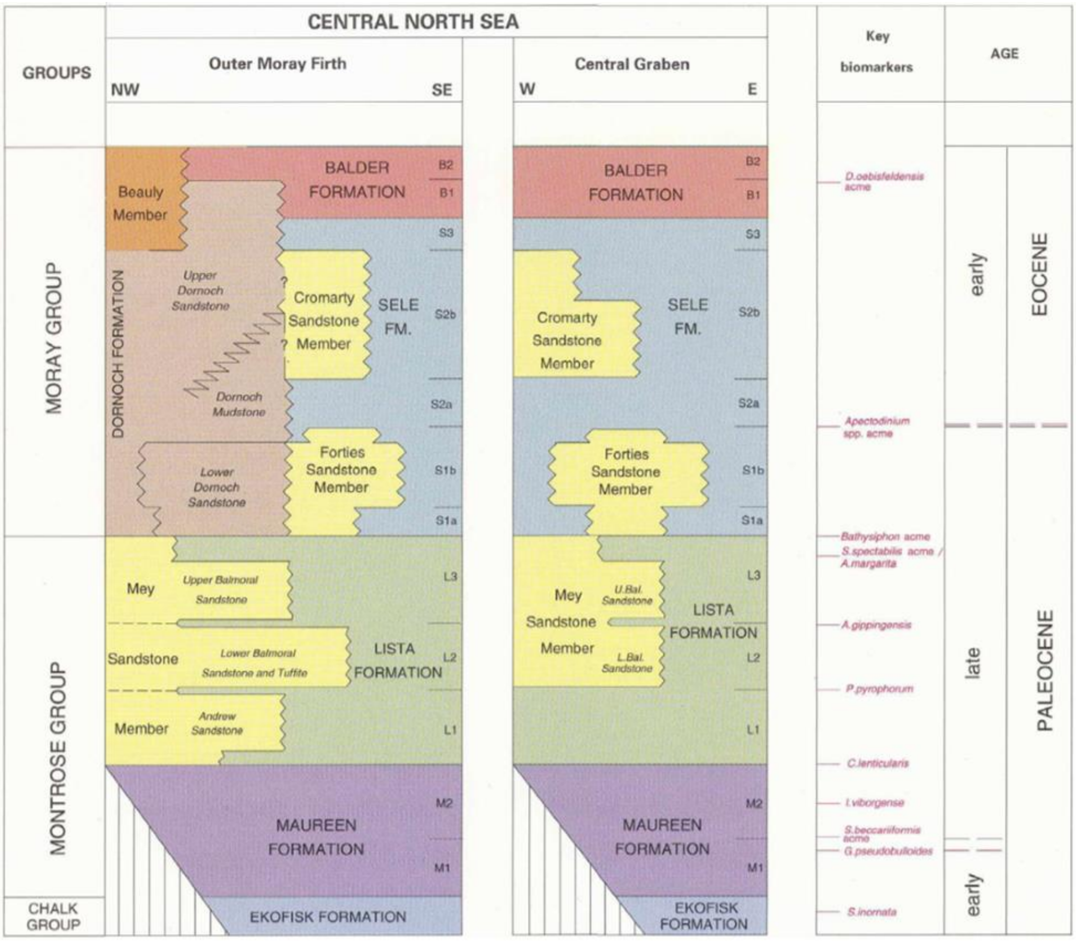

Figure 3. *Lithostratigraphic scheme for the Lower Paleogene (Montrose and Moray Groups) of the Central North Sea (adapted from Knox and Holloway, 1992)*

As it can be seen from the figure 3, the Mey sandstone member consists of three sub-members (Upper Balmoral, Lower Balmoral and Tuffite and Andrew sandstone (note that Andrew member is absent in the Central graben). It is also can be seen that Mey sandstone member was deposited at the same geological time as the Lista formation. It explains by the nature of the deposition processes for two types of formations: high energy turbidites of Mey sandstone and low energy basinal shales of Lista formation.

The topography of the region that was formed before the deposition of the Paleocene turbidites is the key in the control of the sedimentation. The studied area was before accommodated by the pelagic carbonates in the Late Cretaceous. The opening of the North Atlantic triggered the uplift of the Scotland-Shetland region and the movement of the East Shetland Platform as well as rifting of the Central graben in the North Sea. As a result, sediments were sourced from the high relief and were transported in the direction of the basins (Mudge and Copestake 1992).

The Montrose Group associates with the sea-level fall and the uplift of the basin margin. It resulted in the accommodation of turbidites, the fan of the submarine sandstone accumulation. It interbedded with the pelagic mudstone that formed by the relative sea-level rising, flooding of the basin and the sediment cut-off (Milton *et al.* 1990). The transition from Montrose to Moray groups is marked by the cut-off in oceanic microfauna and the change to dark-laminated mudstone. The area of the Outer Moray Firth was in the narrow and land-locked gulf with the limitation to open oceanic circulation. Later Moray group (Forties, Cromarty sandstones) and some of the late Mey sandstone sediments were deposited by the accompanying of the volcanic ash-falls. These ashes were derived from the volcanic sources of the north and north-west of Britain (Morton and Knox 1990).

The Lista formation is represented by the outer shelf to deep-sea basin environments. Hemipelagic mudstone from the deep-sea environment presents the low-diversity fauna and that suggests that basin was in a limited connection to the open ocean. The sand sediments and tuffite units are the subdivision of the Mey Sandstone Member within the Lista formation and it represents the apron of fan deposits (Stewart 1987). Presence of the tuffite speculated to be derived from the eruption of Herbid and Greenland-Faroes provinces (Knox and Morton 1998).

Processes and products

Process (control)	Product (sediments)
1) A low-energy deep water system	1) Basinal shale (hemipelagic mudstone)
2) High-energy submarine gravity flow (turbidity current, debris flow)	2) Fan (turbidites, debrites)

Table 1. *Variations of processes and products that control the deposition in the deep-sea environment of the Central North Sea.*

Turbidite sandstones depend on the source input and the hydrodynamics during the flow. Classic turbidity currents of the Bouma sequence is rarely seen in the Paleocene and Eocene of the North Sea (Stow 1986). Therefore, products of local currents are normally sustained and show the little variation in a range from the fine to medium sand grain size with insignificant fining upwards. One of the reasons for this can be a previous sorting of the sediments on the shelf.

However, some studies in this area suggested that it is more accurate to use the term a gravity flow as the base process to explain the delivery system to deep-water (Normark 1970; Normark and Piper 197; Mulder and Alexander 2001). From the beginning, scientists differentiated two types of end-member transport systems:

1) Debrites – produced by the debris flow and normally presented by high-sediment concentration and cohesive characteristic. It has laminar and weak turbulent flow and significant clay content.

2) Turbidites – produced by lower sediment concentration, non-cohesive and turbulent turbidity current.

This separation can be useful in terms of the assessment of this units by a hydrocarbon perspective, because clay-rich cohesive debrites have a bad reservoir quality, while the sandy turbidites can have a moderate to excellent reservoir quality. However, Mulder and Alexander (2001) proposed the intermediate flow types (hyper-concentrated) that are in the middle of explained types. In addition, Shanmugam *et al.* (1995) suggested the sandstone that is high concentration turbidity current to be as a sandy debris flow. Older works (Mutti and Ricci Lucchi, 1978; Walker, 1978) claimed that the debrite sediments deposited at the base of a slop, while the turbidity current derived sediments deposited deeper toward the basin. More recent theories (Haughton *et al.* 2003; Talling *et al.* 2004, Davis *et al.* 2009) established that debrites are common to be found far from the centre as well on the distal settings and interleaved with turbidity sand units. It suggests that these debris deposits occurred by the same event that for turbidites. It was discussed whether it was formed by co-generated independent flows or from the flow that transformed by less cohesive to cohesive at the process itself. The latter introduced the term hybrid flow for the process and the hybrid event beds for the deposits (Haughton *et al.* 2003). It is important to understand this process and deposits (especially hybrid event beds) because it has resulted in complex, intensively layered hydrocarbon flow units with potentially low communication among it (Davis *et al*. 2009).

The Mey (Andrew) Sandstone Member (The Lista Formation). The most efficient work was done by characterising this sand unit by Kilhams et al. (2012). Axial and lateral route pathways were derived by the seismic and attribute analysis. The axial routing system may split into the westwards and eastwards fairways. It is defined by the topography of the Graben similarly to the Maureen formation. The trend of the lateral systems was explained as not as important by the petrophysical analysis. Cycles within the Mey Sandstone Member have a similar repetition as general for the Paleocene turbidity sandstone members and it was prograding until the late part of the backstepping process. Consequently, these variations underlined the importance and influence of the sea-level curves. Analysis of the core exhibits that the mean size of the grain plays a key role in determining the reservoir quality. It was distinguished that there are two types of sedimentological facies of the local units such as channelized (proximal) and sheet-like (distal) presence and it is similar to the Forties sandstones within the Sele Formation. This work is also mentioned that these sediments barely can be described as classic reservoir basin related floor fans because the influence of the topography on gravity flow route and the several entry points of the sediment in the basin made the architecture of the body complicated.

Methods

The methodology is going to be described by the workflow that has done for this work to further replication of the study. It is important to start with the explanation what data was already provided. After that, the main purpose of the methodology is to list the data collection to generate new results to take them to the discussion. To better represent the structure of the methodology, following work-plan chart is created.

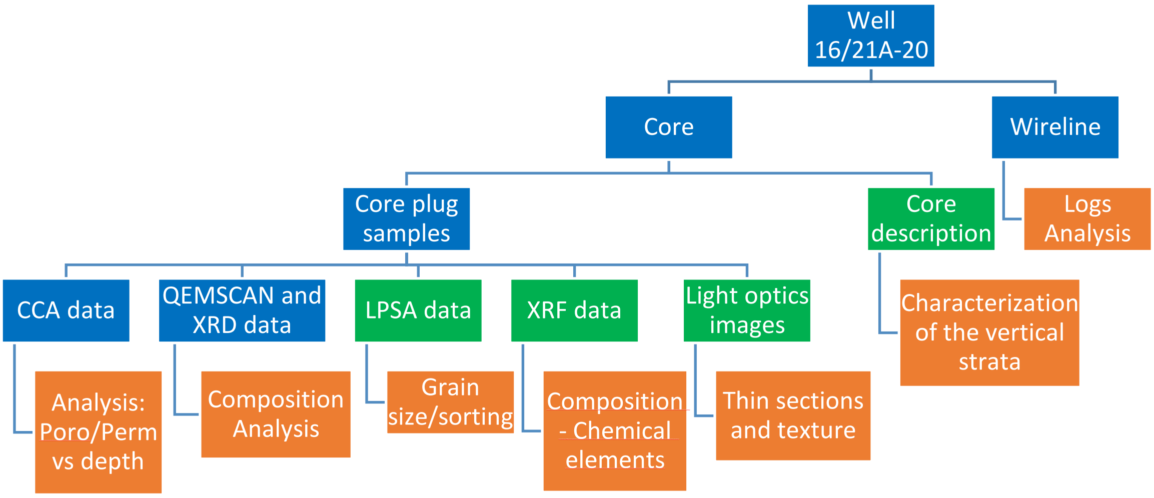

Figure 4. *Work-plan and methodology for the Paleocene Mey Sandstone characterization. Blue colour – previously collected data. Green colour – new data. Orange colour represents what type of results will be generated by previous and new data and will be discussed to answer the main questions this work is specified.*

<u>Previously collected data</u>

In 1990, Sun Oil Britain Limited proposed to directionally drill well 16/21A-20 into the Stirling structure to appraise the reservoir geology and to test the extent of the field. The well was planned to penetrate the Devonian Sandstones and crestal part of the field. The well penetrated the Balmoral Field reservoir of the overlying Mey Sandstone Member (Andrew Formation) which were oil-bearing. Due to operational problems "Ocean Kokuei" was taken off contract and the well was suspended at the top of the Devonian.

Wireline logging was done to this well by Schlumberger during the mentioned appraisal. Dilation Angle (DIL), Bottom Hole Correlation (BHC) and Gamma Ray (GR) were done by first logging run and Lithology Density Tool (LDT), Compensation Neutron Tool (CNT) and Natural Gamma-Ray Spectrometry Tool (NGT) was used by the second logging run. As a result, several wireline logging data were taken that will be shown in the Results section of this report.

Two 8 ½" fibreglass sleeved cores were taken within the Mey (Andrew) formation in order to determine the level of the oil-water contact of the Balmoral reservoir. Core 1 consists of the 12 boxes. Core 2 consists of the 17 boxes.

Core Number	From	To	Feet Cut	% Recovery	Date
1	7272 ft MD	7320 ft MD	48 ft	69	18.9.90
2	7320 ft MD	7369 ft MD	49 ft	100	18.9.90

Table 2. *Two sections summary of the intervals cored, and the recovery achieved. Note that the depth was reflected in the measured depth.*

Core Laboratories were requested to perform a series of conventional core analysis (CCA) measurements, as listed below, on samples from this well.

1. Surface Core Gamma Log (1:200).
2. Permeability – every foot.
3. Porosity – every foot.
4. Grain Density – every foot.

One and a half-inch plugs were drilled with liquid nitrogen at 1-foot intervals in sandstone. The samples were wrapped in 0.04mm thick aluminium foil.

A recent interest of this data was caused by the development of Carbon Capture and Storage (CCS). QEMSCAN (Quantitative Evaluation of Minerals by Scanning Electron Microscopy) analysis and XRD (X-Ray Diffraction) were done and can be seen in the Results section.

<u>Core description</u>

The initial start for the data collection was by the description of the core intervals mentioned above. There are two core intervals (see table 2) – top and bottom. Each one consists of several core boxes. Each core boxes were placed on the table and was described from bottom to top. The most important kit parts for the core description were grain size card and hand lens – to determine grain size of the sandstone and differentiate siltstone and finer grain sediments. Core description sheet was used as the primary evidence of the description. Due to massiveness and homogeneous nature of the sandstone with no visible sedimentary structures, following scale of the description was used – 1:48. One inch in the core sheet corresponds to 4 feet or 48 inches in the core.

Elements in the core description sheet that were observed are: Samples (represents the number of CCA core plug samples to depth), Depth (in feet, measured depth from the well), Core and Box number, Color and staining of the rocks, Cements, Fractures, Graphic Lithology (represents type of the sediment and colored respectively), Grain size and sedimentary structures, Bedset boundaries, Lithotypes (facies), Key surfaces and Remarks column.

<u>Laser particle size analysis (LPSA)</u>

Core plugs that were taken for the CCA analysis left the holes inside of the core. Consequently, these core holes correspond to the depth of the core plugs. This is important because samples will be related to the existing data of core plug depth such as the CCA porosity and permeability. As a result, samples of the sandstone were collected from the sides of these holes by using gentle technic of scraping to take cemented parts of the sandstone. Then, these samples were directed to the geochemical laboratory of the University of Liverpool. To run these samples into the laser particle size analyzer machine, they should be friable and loose. To make them so, following workflow was used. After the sample preparation, all of them were distributed into the small plastic bags and marked correspondingly to the core plugs depth.

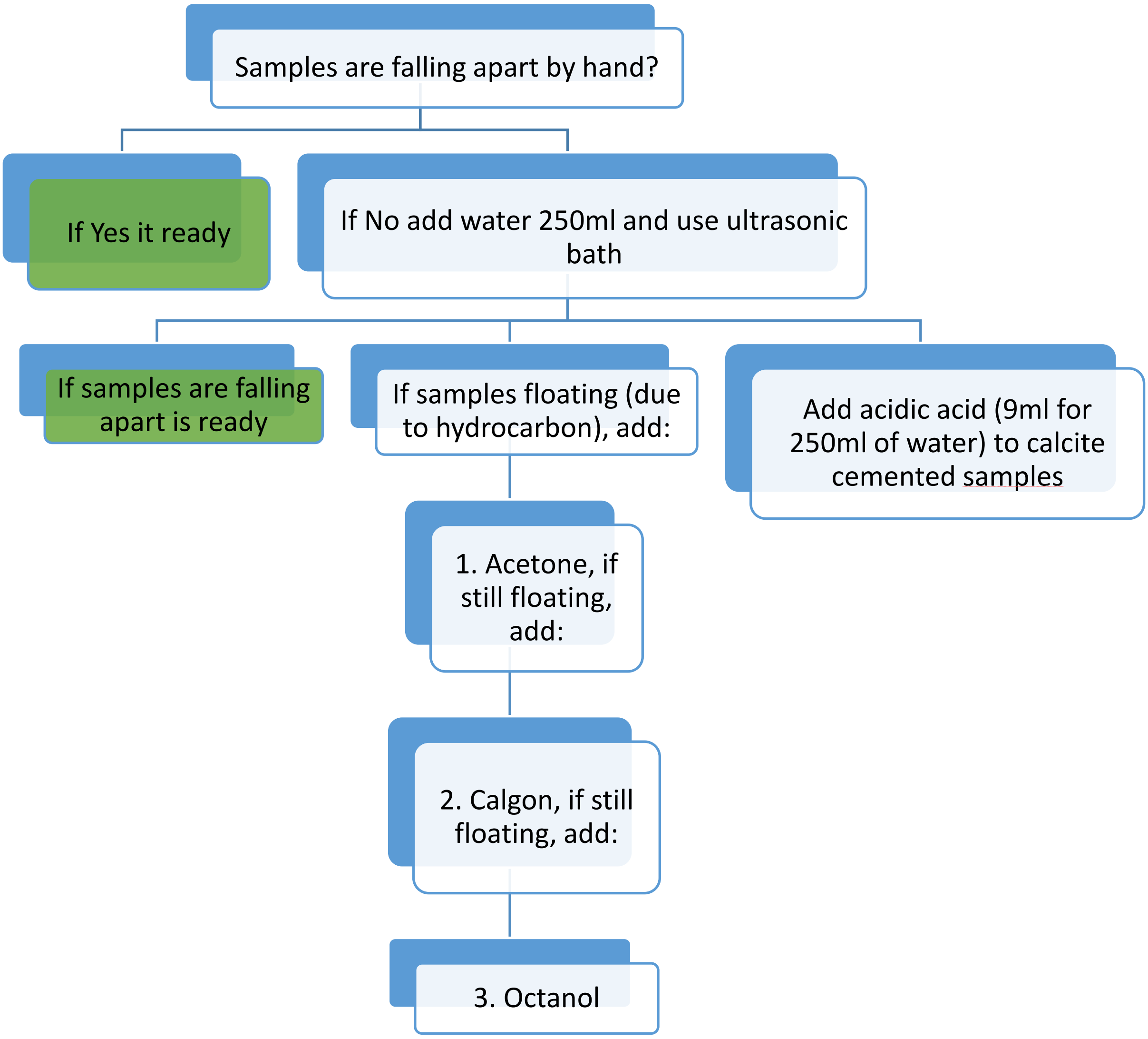

Figure 5. *Preparation of the samples for the laser grain size analysis (LPSA). An ultrasonic bath was used after each addition of Acetone, Calgon, Octanol and Acid.*

The main technology that is in Laser particle size analysis (LPSA) is the laser diffraction method. The forward diffraction of a laser beam by the particles is used to determine their size distribution. The diffraction angle is inversely proportional to particle size, and the intensity of the diffracted beam at any angle is a measure of the number of particles with a specific cross-sectional area in the path of a beam (Eshel *et al.* 2004).

Beckman-Coulter LS 320 was used as the laser diffraction equipment to maintain the samples to provide the grain size/sorting data. Before the loading, samples were featured with additional Calgon to free them from the clay. A value of 7%-12% obscuration is ideal for sample measurement (no more than 15%). Three numbers of the run were determined, and the average was taken to the results.

Results for the grain size analysis were generated by the Microsoft Excel-based programme Gratistat (Blott and Pye 2001). The following samples statistics are then calculated using the method of moments in Microsoft Visual Basic programming language: mean size, mode, sorting (standard deviation), skewness, kurtosis, D10, D50, D90, D90/D10, D90-D10, D75/D25 and D75-D25. Grain size parameters are calculated arithmetically and geometrically (in microns) and logarithmically (using the phi scale) (Krumbein and Perrijohn 1938). Linear interpolation is also used to calculate statistical parameters by the Folk and Ward (1957) graphical method. In terms of graphical representation, the programme illustrates the graphs of the grain size distribution and cumulative distribution of the data and displays the sample grain size on triangular diagram. Samples were analysed together as the programme can take up to 250 samples.

XRF

X-ray fluorescence (XRF) is a fast, low-cost and non-destructive analysis of geochemical composition (Fisher *et al*. 2014). X-ray source emits the x-ray signals that separate the inner and outer shell electrons. After that, the relocation of outer shell electrons is vacated by inner shell electrons resulting in triggering fluorescence. This fluorescence is an emission of Brehmstrahlung x-rays and electromagnetic radiation and the difference between these two electrons. The emission of elements recognizable because a single element corresponds to a unique atomic structure (Mauriohooho *et al.* 2016). Energy dispersive spectroscopy-EDS records the amount of x-ray spectrum energy and indicates a peak line spectrum (Shindo and Oikawa 2002). The measured composition of elements is presented by counts per unit time per unit area (Chawchai et al. 2015), counts rates, ratios of counts and intensity of elements (Rothwell et al. 2006). This technique was adapted to use in determining the chemical compositions of the sedimentary rocks (Jenkins 1999, Young *et al.* 2016).

Elements that can be analyzed by the portable XRF device are: Al, Si, P, S, Cl, K, Ca, Sc, Ti, V, Cr, Mn, Fe, Co, Ni, Cu, Zn, As, Se, Rb, Sr, Zr, Nb, Mo, Pd, Ag, Cd, Sn, Sb, Te, Cs, Ba, Hf, Ta, W, Re, Au, Hg, Pb, Bi, Th, and U. All these elements have a corresponded them detection limit and an error measure that are a function of the rock matrix and time analysis. Detection limit for light elements (Al, Si) is higher than for the heavier elements (Fe, Ti) because of the lower energy of the x-ray emission from the lighter elements. Si and Al, however, are known as major elements in most sedimentary rocks and their error value considers acceptable. Hydrogen, carbon, nitrogen, oxygen, fluorine and sodium are excluded from the list because secondary x-rays are below the detection limit (Worden 2019 [in press]).

Samples for the XRF analysis were chosen on the base of the core plugs that were previously used for the CCA data. All the core plugs were placed one by one on the mobile test stand that was in the connection to the XRF equipment. Due to mobility and portability of the equipment, measured data were taken in the core itself for the absent core plug points.

Portable XRF tool consists of an x-ray source paired with Si-PIN and CdTe detectors (Young *et al*. 2016). This tool offers real-time chemical and chemostratigraphic data, portability, relatively low-cost, convenient size of equipment and highly accurate measurements (Weinforf *et al.* 2012). For this work, Thermo Scientific Niton XL3t GOLDD+ device was provided by the University of Liverpool. This tool uses 9-50kV, 0-40 µA Au anode x-ray source. Additionally, technology of the Niton tool records more than 180000 detectors per second and utilizes 2.5x more signal detections. Settings for the equipment were chosen based on the uncertainty test. Different times were used and then plotted on the graph to use the optimal time range (see figure 6). Element range settings were chosen in total 160 seconds as follows: Mode: Test All Geo; main range: 30 sec; low range: 30 sec; high range: 30 sec; light range: 60 sec + 10 seconds for the regulation. Measurements from the XRF tool were recorded by provided software - Niton Data transfer (NDTR) 6.5 and resulted in the Microsoft Excel spreadsheet.

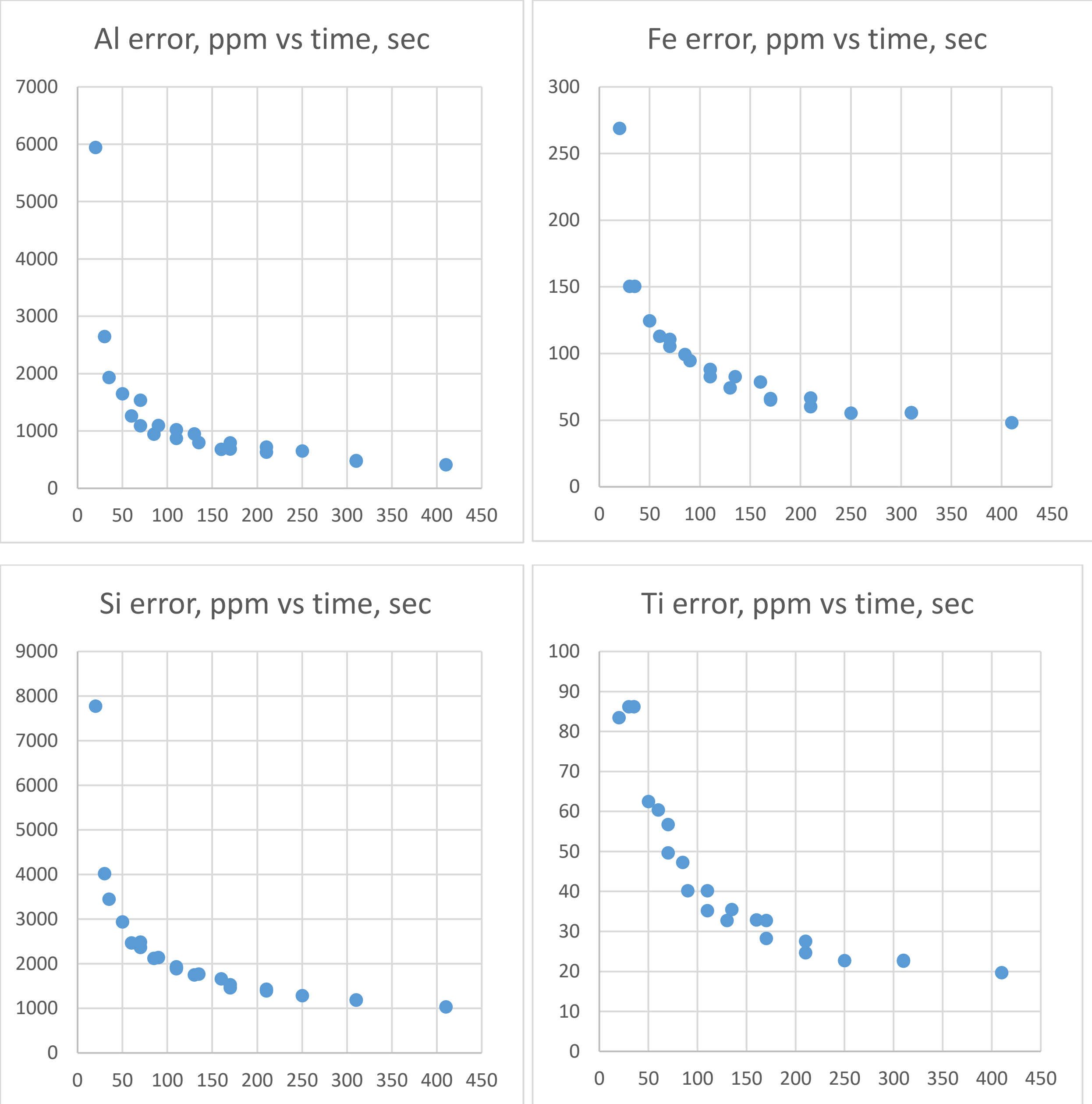

Figure 6. *Uncertainty test for 4 main elements (Al, Si, Fe, Ti). 160 seconds were chosen as mentioned due to time efficiency and a relative error value.*

Light optical microscopy

Polished thin sections were provided to analyze it through the microscope to assess the mineralogical composition of the studying sandstone. The microscope that was used is the Olympus BX51. Software that was utilized to create images is cellSens. Light optics was used after the primary interpretation of the wireline, CCA, LPSA and XRF data to find the needful features in textures and mineralogy of the Paleocene Mey sandstones.

To summarize all the samples for different methods, the table below is created. It will be helpful to understand following results section. Some samples that were used for CCA have been destroyed due to high shale presence or calcite cementation.

Sample Number	Depth	CCA	LPSA	XRF	Light optics	QEMSCAN and XRD
1	7272					
2	7273					
3	7274					
4	7275					
5-10	7276-7281					
11	7282					
12-14	7283-7285					
15-16	7286					
17-20	7288					
21	7292					
22-24	7293-7295					
25	7296					
26	7297					
27-29	7298-7300					
30	7301					
31	7302					
32	7303					
33-34	7304-7305					
35	7320					
36	7321					
37-38	7322					
39	7324					
40-44	7325-7329					
45	7330					
46-48	7331-7333					
49	7334					
50	7335					
51-53	7336-7338					
54	7339					
55-63	7340-7348					
64	7349					
65-66	7350-7351					
67-68	7352-7353					
69-71	7354-7356					
72	7357					
73-74	7358-7359					
75	7360					
76	7361					
77	7362					
78	7363					
79	7364					
80-82	7365-7367					
83	7368					

Table 3. *Representation of samples and methods for which they were used. Note that depth of samples corresponds to every foot and some of them were combined for this table (55-63, 7340-7348).*

Results

As it was mentioned above, results for this work will have two different types: previously collected data (Wireline data, CCA data and QEMSCAN data) and new data (Core description, LPSA data, XRF data and Light optics images).

Wireline data

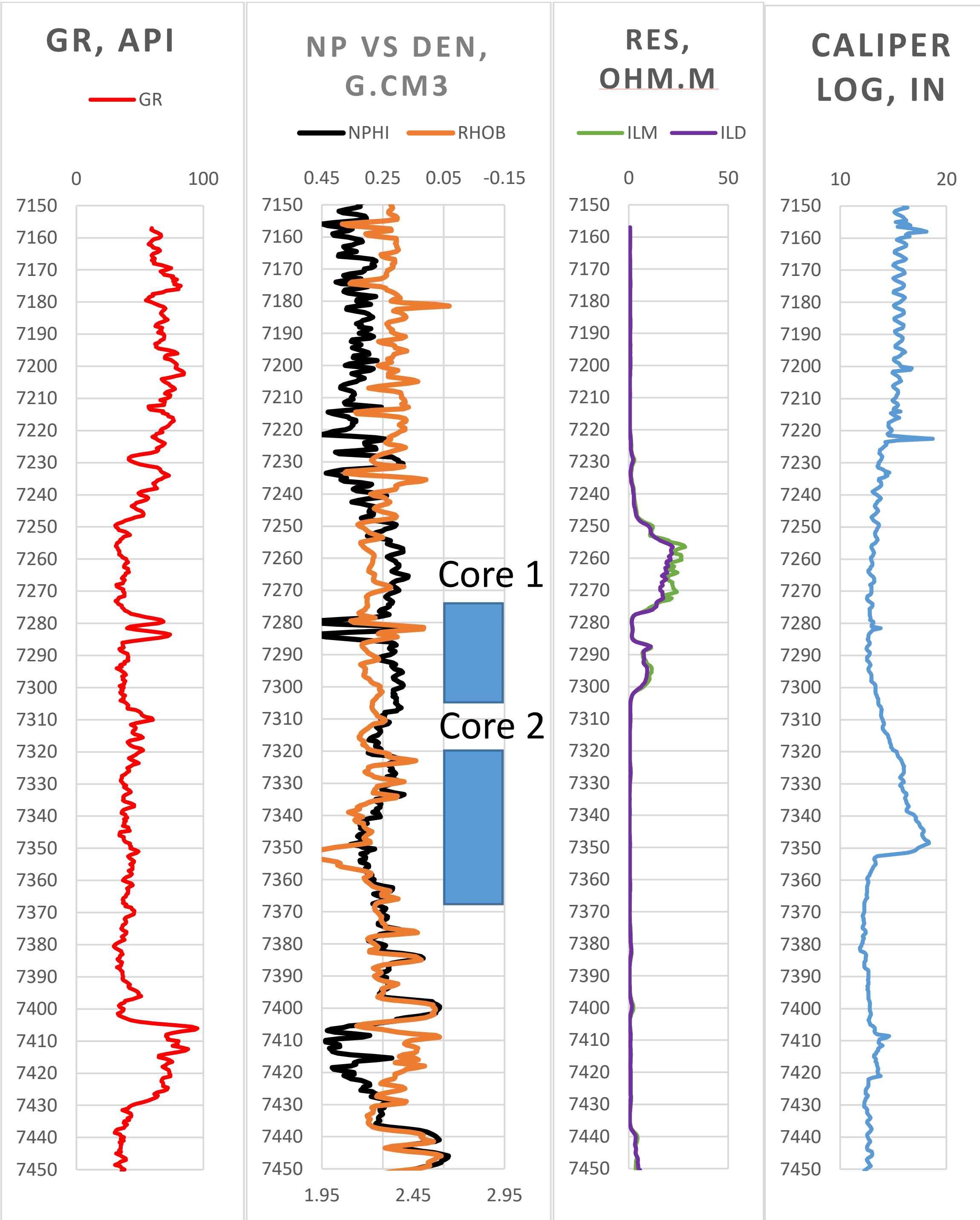

Figure 7. *Wireline log data of Gamma Ray (GR), Neutron Porosity vs Density log (NP vs DEN), Resistivity log (RES) of Medium (ILM) and Deep(ILD) and Caliper Log (CALI) with the reference to Core 1 and Core 2.*

Core description

As it was mentioned in the Methods section, Core 1 (top section) and Core 2 (bottom section) were described and represented in core description sheets below. Core 1 or top section is presented by sediments from sandstone to claystone. Claystone is seen on top (7272-7274.5ft) and as interbedded thin clasts (no more than 8-10 inches) in between 7282-83ft, 7297-7298ft and 7299-7300ft. Comparing to claystone, sandstone is dominated in the core 1 and was described as moderately consolidated, poorly cemented, moderately sorted with fine-medium sand grain size and visible intergranular porosity. It is also seen with brown to dark yellowish colour with recognizable hydrocarbon odour. Vertical variation in sandstone is minor. Consolidation of the sand is poorer as it goes to the bottom. Siltstone and very-fine sandstone are also seen in 7297ft, 7300-7301ft that are in association of gold-like nodules (can be pyrite). At the lowest part of the core (7303ft) preferable oriented mud drapes and black traces are marked.

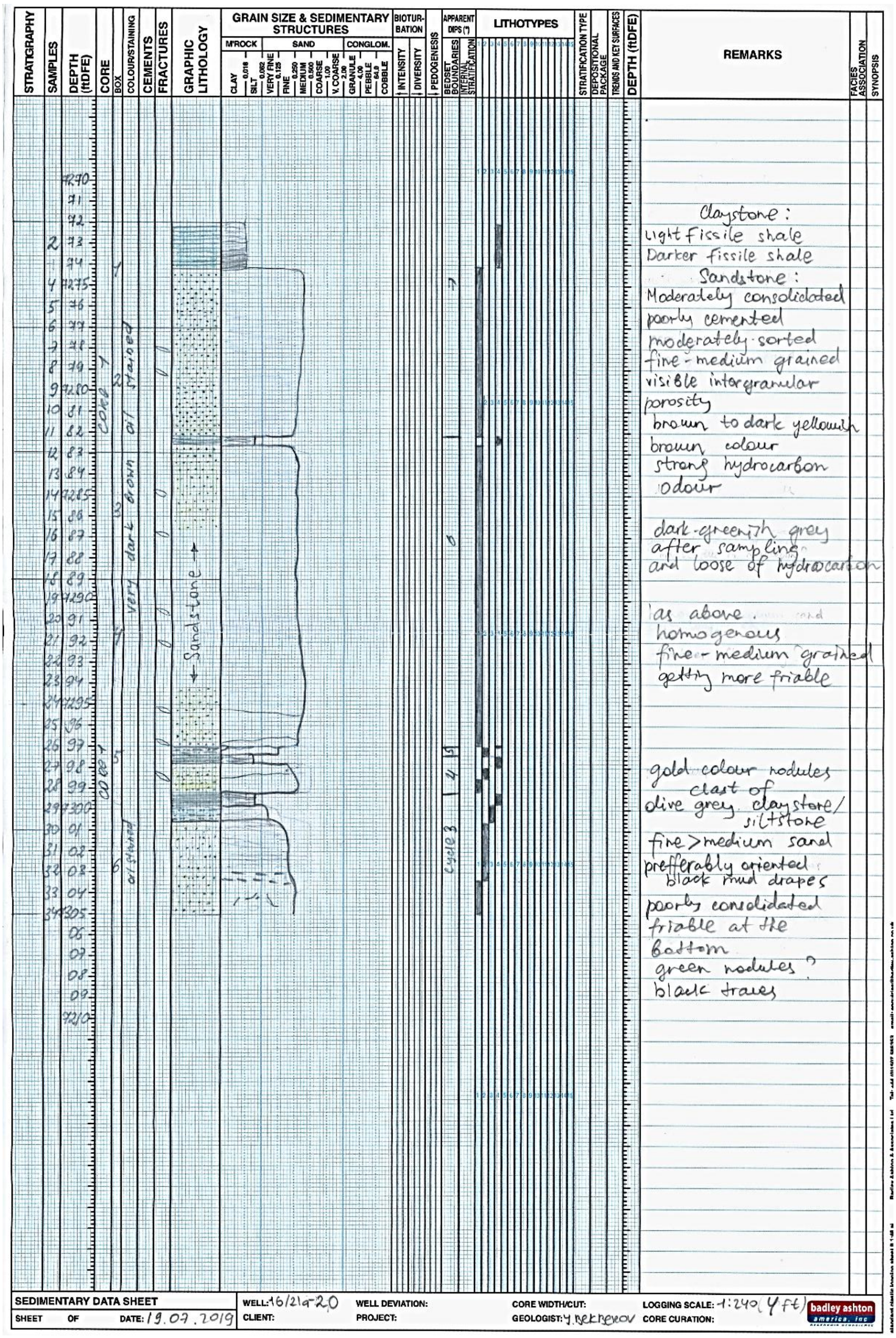

Figure 8. *Core 1 description. 6 pair of core boxes were examined. References to sample depth were seen from the core (parallel to core plug drilled holes). Some fractures were thought to be artificial due to absent of cementation and horizontal distribution. Claystone on top and interbedded claystone clasts are seen. Fine-medium dark brown sandstone dominates the whole section. 4 lithotypes were recognized with bed boundaries. Further interpretation will be presented in the Discussion section.*

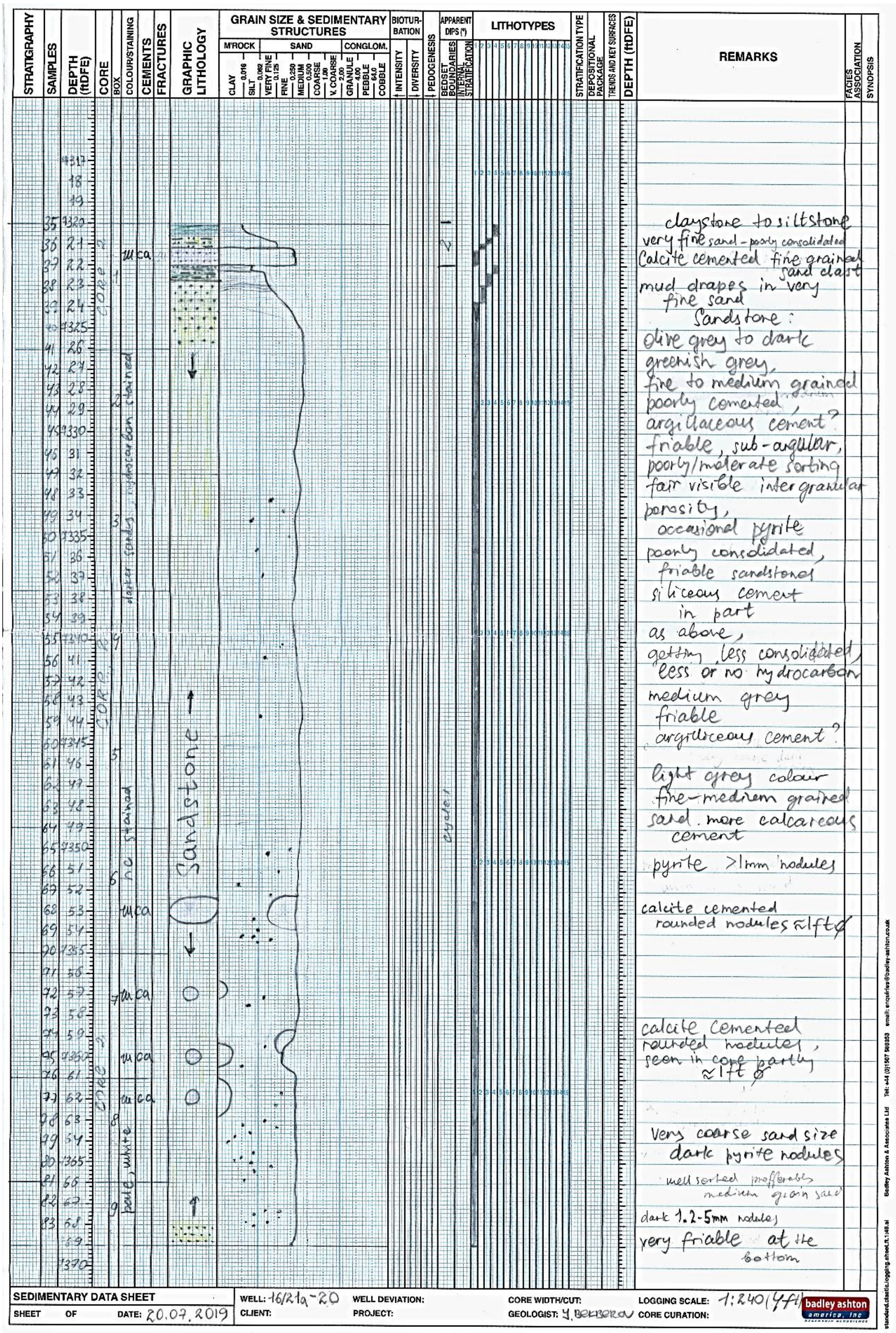

Figure 9. *Core 2 description. 9 paired boxes were examined and described. Variation from claystone to sandstone is seen on top (with a pale grey cemented clast), rest of the core is dominated by the grey homogeneous sandstone. Black opaque coloured pyrite and pale grey cemented nodules are the main features in the bottom part of the core.*

Core 2 is presented mostly by sandstone. Thin claystone to siltstone clast is repeated twice on the top of the core (7220-21ft and 7222-7223ft). In between cemented fine-grained sandstone clast is seen on 7221-7222ft. Sandstone is olive-grey to dark-greenish grey, fine to medium sand grain size, poorly cemented with possibly argillaceous material, friable, from poorly to moderate sorting, Variation in composition of sandstone is visible minor. On lower part of the core cemented nodules are seen approximately 1 foot long, rounded with pale grey/white colour. Pyrite nodules 1.2-5mm on the bottom (7252-7269ft) and approximately 1 mm in the middle section (7330-7352ft) are common.

<u>CCA Porosity/Permeability, LPSA and XRF data</u>

For better representation, a combined table was created below including previously collected CCA data (helium porosity and horizontal permeability) and newly collected data such as LPSA data (mean grain size and Folk and Ward method derived logarithmic sorting) and XRF data (Ti, Ca, K, Al, Si, Fe, S and Cl).

Sample	**Depth, ft**	**CCA Por, % (He)**	**CCA Perm (H), D**	**MEAN, µm**	**SORTING, φ**	**Ti, ppm**	**Ca, ppm**	**K, ppm**	**Al, ppm**	**Si, ppm**	**Fe, ppm**	**S, ppm**	**Cl, ppm**
S2	7273					15267	3338	30181	136828	286057	57628	12010	3758
S4	7275	24.6	1371	322	0.92	782	7364	9429	17895	439164	3130	1371	< LOD
S5	7276	27.3	1415	268	1.74	1470	17273	13431	34463	387073	4846	2530	196
S6	7277	26.5	1134	317	1.01	1572	13380	13748	37663	387359	6164	5130	93
S7	7278	26.5	1107	288	0.97	1167	3112	12394	31544	403097	3280	2749	233
S8	7279	26.2	841	299	1.08	864	5571	12846	32833	410770	8345	11376	330
S9	7280	25.5	529	263	1.36	1220	8370	14690	36980	365436	20775	33845	119
S10	7281	24.6	493	288	1.16	1569	682	12981	31054	420705	16486	16943	216
S11	7282	27.1	1002	232	1.07	1615	686	15040	45343	390808	3694	3325	123
S12	7283	26	928	241	1.08	952	3781	12930	33225	421109	5094	13198	308
S13	7284	25.7	795	259	1.06	1040	9758	10983	34179	418125	3482	6053	902
S14	7285	25.3	800	256	1.23	1589	3511	14754	46736	392575	3874	5591	1108
S15	7286	28.2	659	253	1.07	1454	506	13029	37035	409356	3539	3144	1014
S16	7287	24.4	563	254	1.19	1168	448	10728	34106	440521	2985	3242	332
S17	7288	23.4	517	271	0.95	1386	1436	10459	38687	393429	2673	5512	3543
S18	7289	22.9	511	267	1.12	1260	457	10152	31255	426795	2568	2128	1084
S19	7290	23.2	519	280	1.16	1172	5350	12546	51479	387950	3358	3569	2012
S20	7291	23.5	474	276	1.12	1137	4447	9180	39453	389934	2894	5322	20672
S21	7292	23.3	511	294	0.99	1435	387	12672	38867	425732	3921	4174	128
S22	7293	23.7	524	275	1.24	1322	5769	12597	43082	418113	3685	3377	1490
S23	7294	24.1	655	310	1.06	978	721	11866	39797	442112	3282	2933	1103
S24	7295	24.3	653	293	1.13	1096	6131	11168	37136	425429	3255	2283	853
S25	7296	24.7	765	304	1.06	948	376	10763	25302	451474	2837	2845	81
S26	7297	25.8	587	295	1.12	1193	8745	11183	29942	406450	3730	12217	506
S27	7298	25.6	571	258	1.45	1160	3784	12058	46669	366357	23513	33210	988
S28	7299	23.9	467	262	1.36	987	6283	11692	39534	410044	15946	25910	948
S29	7300	20.9	25	124	2.15	1337	19032	14060	46408	361650	4474	10017	1499
S30	7301	24.4	222	244	1.63	1251	861	13958	41300	423565	4207	3148	114
S31	7302	24.5	143	177	1.52	2755	13259	17955	80549	326474	12635	24504	2852
S32	7303	28.4	717	227	1.37	2241	709	19227	74993	347182	14021	14729	45
S35	7320			29	1.82	6486	10568	24589	95057	237818	34798	21303	3589
S36	7321												
S37	7322			46	2.34	1937	153294	11448	41091	210091	12047	7934	5097
S38	7323			115	1.71	4041	3423	21447	69697	301192	22558	15669	4825
S39	7324	26.7	482	207	1.63	2104	1100	17438	71434	374799	12289	13448	86
S40	7325	25.6	500	299	1.90	2084	10396	13936	55170	341972	12583	28451	< LOD
S41	7326	25.3	327	304	1.60	1444	23180	15024	67593	304919	8916	36954	2146
S42	7327	25.8	436	318	1.97	2462	10779	13891	75348	333127	14401	24144	219
S43	7328	24	247	366	1.68	2457	7589	14096	63251	377990	11485	19183	525
S44	7329	26.2	445	269	2.01	1875	9955	15460	55919	372048	10746	19882	924
S45	7330	24.9	357	321	1.77	2569	3574	14908	67455	342856	16254	19528	78
S46	7331	24	235	218	2.01	2218	16876	14806	82298	345776	11885	10437	6069
S47	7332	23.8	259	253	1.99	2595	12235	14049	80551	335209	15906	13154	1858
S48	7333	23.5	243	315	2.10	2310	11561	14959	69678	367536	13224	13724	1454
S49	7334	26	381	263	1.68	2031	1143	14273	62377	376666	11134	16256	309
S50	7335	24.3	219	282	1.52	2515	4586	15774	73647	356515	14101	17662	1022
S51	7336	23.6	133	263	1.90	1712	27228	11728	48296	320735	11520	47719	760

S52	7337	24.8	312	246	1.83	2535	5120	14328	61423	312783	12454	17438	329
S53	7338	25.3	508	336	1.77	1992	5924	12342	55827	359364	11444	19059	2024
S54	7339	25	430	285	2.12	2184	4580	14165	57209	345626	11310	16289	74
S55	7340	25.8	468	339	1.69	2666	8168	13712	69575	312080	12621	21121	786
S56	7341	25.8	439	306	1.72	2699	6464	15751	57226	316279	10976	22146	332
S57	7342	24.6	412	300	1.93	2874	2944	13915	66095	294891	14784	17849	330
S58	7343	24.6	396	328	2.20	2324	4003	13605	54114	325415	11376	18444	< LOD
S59	7344	25.1	426	364	1.99	2726	5902	12191	65408	279999	12257	20496	1064
S60	7345	24.5	314	346	2.47	2412	13776	14187	63552	282019	11874	20364	831
S61	7346	23.6	433	306	1.92	2492	5949	14620	69861	343721	13851	20484	1409
S62	7347	24.6	495	337	2.08	1639	16663	10510	54780	347663	8587	29095	2623
S63	7348	24.1	352	333	2.10	2048	27995	10953	50264	281270	10392	42899	721
S64	7349	25.2	626	302	1.95	2330	5833	13672	61035	351932	12058	20555	327
S65	7350	23.6	367	289	2.12	1930	8505	13411	53496	358793	11709	24079	276
S66	7351	24.1	248	224	2.01	2199	4516	13817	82856	340529	16901	20924	4868
S67	7352	23.9	383	295	2.13	2292	5483	13669	61605	385152	11887	19238	279
S68	7353	3.7	0.23	286	1.06	1047	202494	10181	27975	290232	7536	4434	224
S69	7354	23.4	287	269	2.00	1841	2647	13590	52419	400722	14327	15916	183
S70	7355	23.1	186	226	2.25	2056	5795	15754	67156	363903	14582	13630	267
S71	7356	22.4	188	246	1.57	2445	7913	13480	69267	376110	13653	20964	1057
S72	7357			332	1.32	687	95858	5520	20419	123146	6593	22938	118814
S73	7358	22.4	189	255	1.25	1900	18821	12102	51262	333527	13062	41632	806
S74	7359	22.7	177	278	1.88	1908	9279	13658	77079	329782	14192	26280	2484
S75	7360			192	1.01	841	132666	10219	29188	277505	6305	30407	1657
S76	7361	20.9	159	286	1.47	2150	3071	15773	66064	386285	12103	14607	361
S77	7362			332	0.86	1072	199738	8256	29298	268363	5490	4301	3260
S78	7363			272	1.92	2984	2048	14440	62937	308066	14431	13924	4046
S79	7364	24.6	272	264	2.02	2476	4031	14110	75233	326978	16668	23536	158
S80	7365	24	259	248	2.03	2126	5747	13323	63416	381186	13021	17027	1122
S81	7366	22.5	221	302	1.31	2485	5246	13717	73483	377291	11584	15818	1226
S82	7367	23.2	197	225	1.79	3053	2096	16043	64339	376690	13189	11961	212
S83	7368			246	1.90	3076	4385	14015	69033	279926	10058	9535	2775

Table 4. *Combined table of CCA, LPSA and XRF data.*

QEMSCAN and XRD

Depth (ft)	Porosity (%)	Quartz (%)	Plagioclase (%)	K-Feldspar (%)	Calcite (%)	Siderite (%)	Smectite (%)	Kaolinite (%)	Muscovite (%)	Pyrite (%)
7275.00	32.31	86.23	2.84	7.06	0.62	0.21	0.86	0.81	0.39	0.33
7282.00	36.76	83.83	3.3	8.06	0.01	0	1.3	1.83	0.42	0.52
7286.00	33.62	85.83	2.86	7.26	0	0	1.03	1.53	0.38	0.48
7287.00	31.79	86.72	2.46	6.58	0	0	0.94	1.55	0.36	0.67
7292.00	31	85.88	2.73	7.06	0	0	0.97	1.6	0.4	0.59
7296.00	31.26	85.55	2.65	6.91	0	0	1.09	1.55	0.34	0.8
7297.00	32.96	84.83	3.29	7.12	0	0	1.26	1.35	0.51	0.44
7301.00	31.11	82.02	3.84	7.96	0.01	0	1.82	2.05	0.35	0.69
7303.00	39.12	70.95	6.69	9.52	0	0	1.46	4.65	0.38	5.04
7324.00	35.38	71.81	6.97	10.14	0	0	0.96	4.79	0.35	3.93
7330.00	29.62	72.01	5.76	9.07	0.06	0	0.83	5.27	0.24	5.25
7334.00	31.21	72.5	5.5	9.13	0.02	0	0.98	5.17	0.24	4.93
7335.00	32.94	72.29	6.56	8.72	0	0	1.49	5.11	0.44	3.68
7339.00	29.56	73.59	6.35	8.66	0	0	0.96	4.67	0.37	4.23
7349.00	29.83	73.59	5.55	8.61	0	0	0.86	4.75	0.25	5.08
7352.00	27.77	72.49	5.67	8.59	0	0	0.87	5.29	0.3	5.63
7353.00	1.11	41.11	4.34	7.24	41.08	0.02	1.3	1.91	0.26	1.5
7361.00	25.8	72.5	5.24	7.92	0.01	0	1.08	5.46	0.31	5.59
7364.00	31.56	72.9	5.72	7.79	0	0	0.83	5.84	0.28	5.13

Table 5. *Previously collected results from QEMSCAN and XRD. Dolomite, other carbonates, glauconite, biotite, rutile, ilmenite, Fe oxides, apatite, zircon, chlorite, others and unclassified are absent from the table due to insignificant concentration. Pale yellow and pale green colour were added to differentiate the top (core 1) and the bottom (core 2) sections of the core.*

Light optics

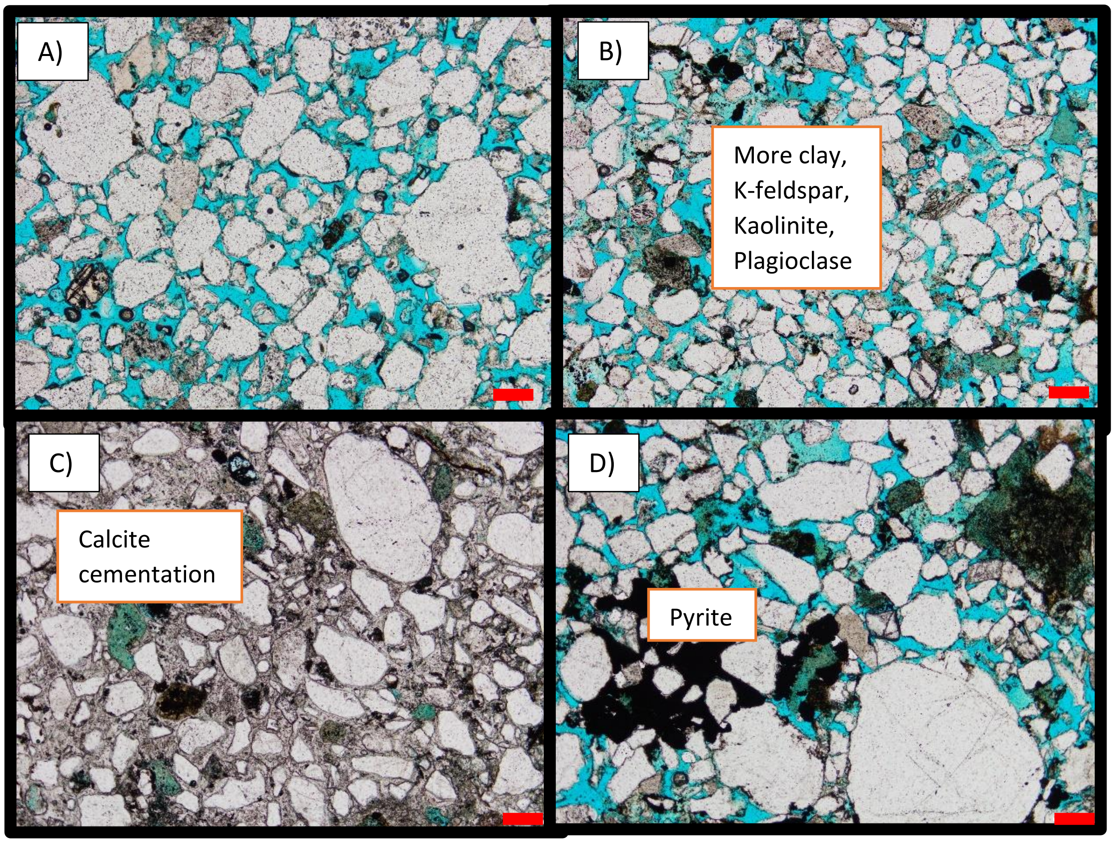

Figure 10. *It is impossible to include all thin sections and these images were chosen to represent the main features in studying reservoir rock. A) S4-7275ft exhibits cleaner pore spaces and better sorting of the grains. Mainly quartz, with rare presence of K-Feldspar and Plagioclase. B) S39-7324ft shows more clay minerals such as K-feldspar, plagioclase and kaolinite that is almost absent from the upper part of the core. C) S68-7353ft is derived from the cemented nodule and correspondingly pore spaces are filled by cement. Noted that pyrite and kaolinite are less common in cemented nodule comparing to the neighbouring intervals. D) S64-7349ft represents the pyrite nicely and pyrite is common to see in the lower intervals as well as kaolinite. Furthermore, sorting is poorer comparing to the upper part of the core. Length of the red line corresponds to 200µm.*

Discussion

What is the vertical stratigraphy?

The core consists of two section top (7272-7305ft) and bottom (7320-7369ft). It must be mentioned that the middle section between these sections (7305-7320ft) is absent from the core. The sandstone of top section (Core 1) is characterized as dark brown coloured with oil odour what makes to think that it is a hydrocarbon-bearing sandstone. It confirms previous work that was done in industry to determine oil-water contact (OWC) that is found to be at 7300ft. Apart from that, sandstone is described as moderately sorted, poorly cemented (friable), fine-medium grains size with visible intergranular porosity. It leads that the sandstone has the quality of reservoir rock. The only negative feature that is seen in this section is the claystone (with low permeability) clasts at 7272-7274ft, 7282.5ft, 7297.5ft, 7299.5 ft what can affect the vertical permeability between porous intervals.

Bottom section (core 2) is more dominated by sandstone with two claystone clasts found on top (7320ft, 7222ft). Sandstone is slightly different from the top one and has grey colour and more argillaceous cement, but again it is poorly cemented and friable. However, cemented clast of calcite found between two claystone clasts (7221ft) and calcite-cemented nodules are recognized in the lower part of the core 2. Additionally, presence of pyrite is found as pyrite nodules 1-5mm with high concentration on the lower part.

Generally, comparing two sections of the core in terms of sandstone, it has minor variation. Fine-medium sand grain size with no visible sedimentary structures and with no obvious difference in texture. As the depositional environment of this age and location corresponds to the deep-water environment, there two variations of sediments: hemipelagic mudstone and turbidite sandstone. Lithotypes were differentiated in four types and can be seen from the core description (figure 8, 9) as 1-fine-medium sandstone, 2-very fine sandstone, 3-siltstone, 4-claystone(mudstone). Turbidite sedimentation is interrupted by low energy deposits of fine grained hemipelagic shales. Therefore, bedset boundaries between every turbidite event were recognized by the top of claystone clasts. In terms of the type of the turbidite events (Haughton 2006), mostly all of sandstone seen is likely to be non-cohesive high-density turbidity current as it has sharp transition from the fine-medium sandstone to claystone without smooth shift and sedimentation of very-fine sand and silt. Some non-cohesive low-density turbidity current behaviour can be seen in thin sandstone events. Kilhams (2012) recognized four facies by comparing core-based studies of the Mey sandstones (O'Connor and Walker 1993; Davis et al. 2009): amalgamated sandstone, sand-prone heterolithics, mud-prone heterolithics and hemipelagic mudstones. Because heterolithics were not seen in the core, amalgamated sandstone and hemipelagic mudstones are two facies that can be related to in this core. More than this, hemipelagic mudstones that were seen in thin clasts can correspond to the description of the cap for the amalgamated sandstone. As a result, interpretation of the vertical stratigraphy is characterized by the sedimentation of amalgamated sandstones on each other. Moreover, this facies was associated with the main period/route of sand input into the basin (as repeated high-density flows). However, it is hard to tell from the one well to what it relates: to the proximal area distributary channels or distal area sand-rich sheets (Kilhams 2012).

How does CCA data relate to stratigraphic position?

Relationship to stratigraphy is seen in figure 11. Porosity and Permeability from CCA data are seen higher on the top but differently for each index. Variation in porosity is minor. Thin claystone clasts do not affect the CCA porosity (because it derived in 1foot length and can be between the points) but can affect the vertical permeability. Change in trend on permeability from 1000 to 500mD and backwards (7280ft) and low value of permeability in 7300ft can be influenced by these clasts. What controls the CCA permeability on the bottom part of the core except the carbonate nodules is unknown from the stratigraphic characterization. Calcite cemented rounded nodules can affect the net-to-gross ratio more than vertical or horizontal permeability.

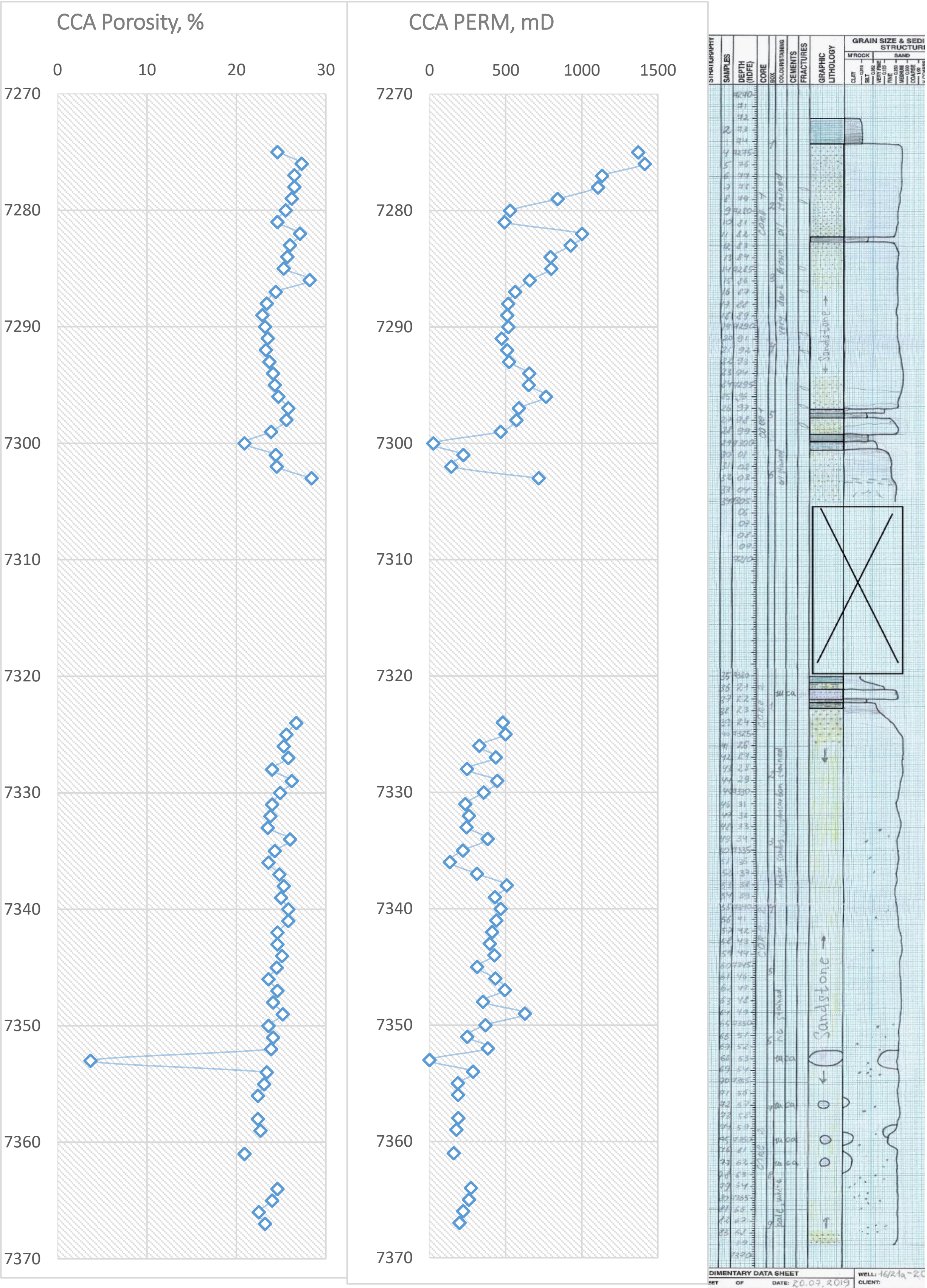

Figure 11. *CCA data vs stratigraphy derived from core description. Porosity is slightly variable and increasing from 20% on the bottom to 26-27% on top. Permeability higher on the top than on the bottom with high difference. Calcite cemented nodule on 7355ft affected porosity and permeability.*

How does grain size/sorting vary with stratigraphic position and CCA?

According to the data derived from LPSA and CCA, we can plot CCA porosity, CCA permeability vs grain size and sorting. Porosity shows less dependency on grain size as all CCA porosity data were derived from the similar grain size sandstone. However, the sorting shows that its control on permeability is significant.

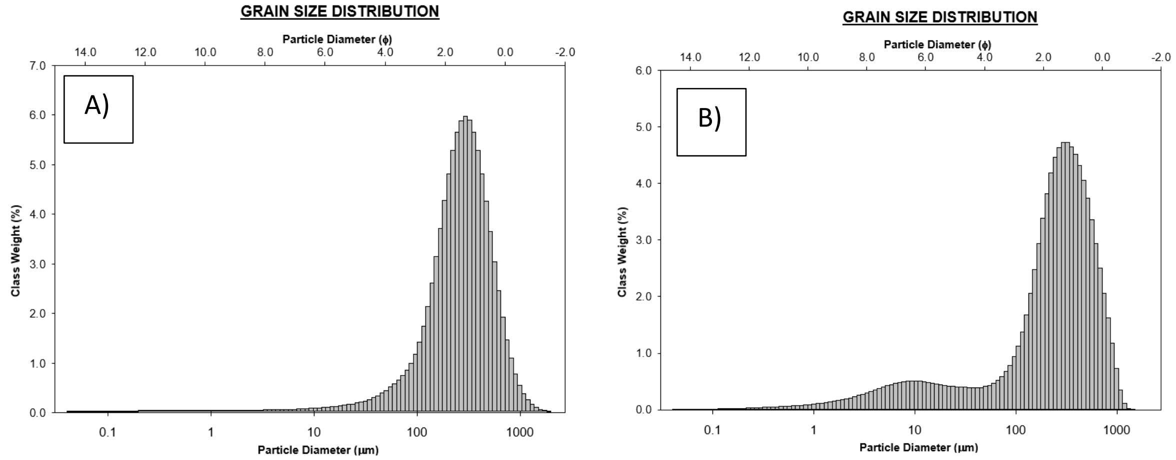

Figure 12. *Grain size distribution for A) S6-7277ft presents the top section of the core (core 1) and shows that sorting of the sands is better with absence of very fine particles. B)S64-7349ft presents the bottom section of the core (core 2) and has more presence of clay and silt size particles resulting in poorer sorting.*

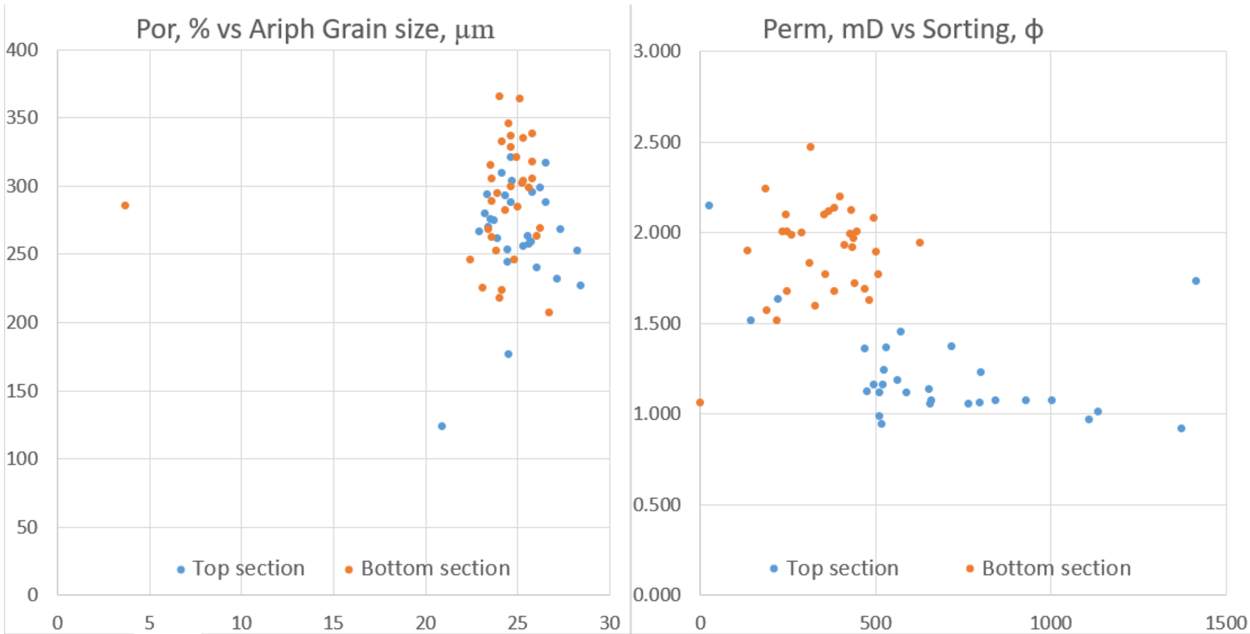

Figure 13. *Two plots represented CCA data vs grain size and sorting. On the left plot relationship between CCA porosity and geometric grain size is presented with minor porosity dependence from grain size within the fine-medium sandstone variation. On the right figure relationship between CCA permeability and Folk and Ward sorting represents that sorting is the main control on permeability. It is also seen that the top section has better values than bottom one.*

How does chemistry relate to the stratigraphic position and CCA?

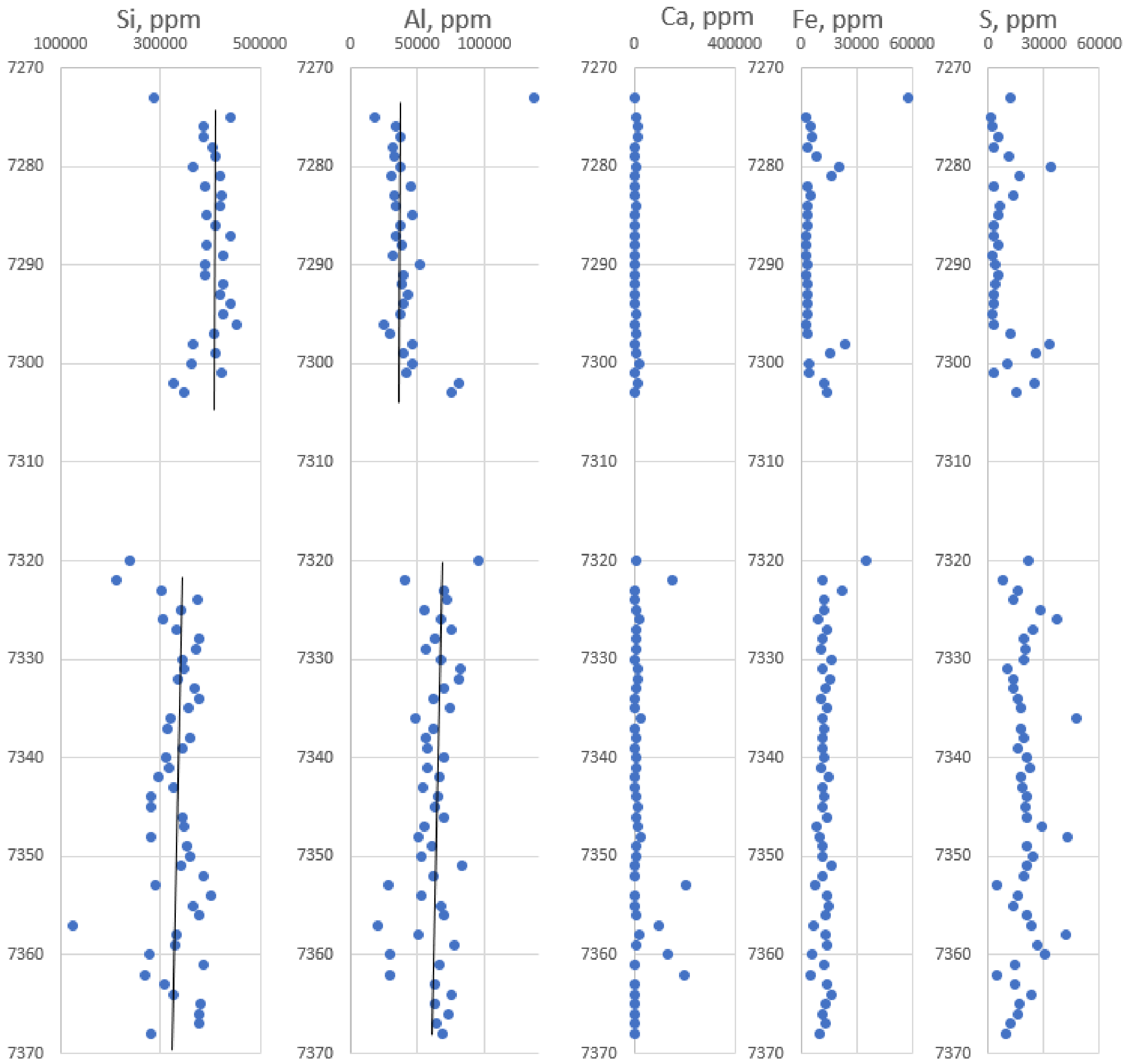

Figure 14. *Si, Al, Ca, Fe and S versus depth. Chemical elements reflects the stratigraphy: Si shows that upper part (core 1) has higher presence of quartz than bottom one (core 2); Al has more values on the bottom core and can reflect the dependency on clay composition; Ca strongly corresponds to calcite cemented intervals; Fe can also be influenced by clay minerals, but with S can show the pyrite minerals.*

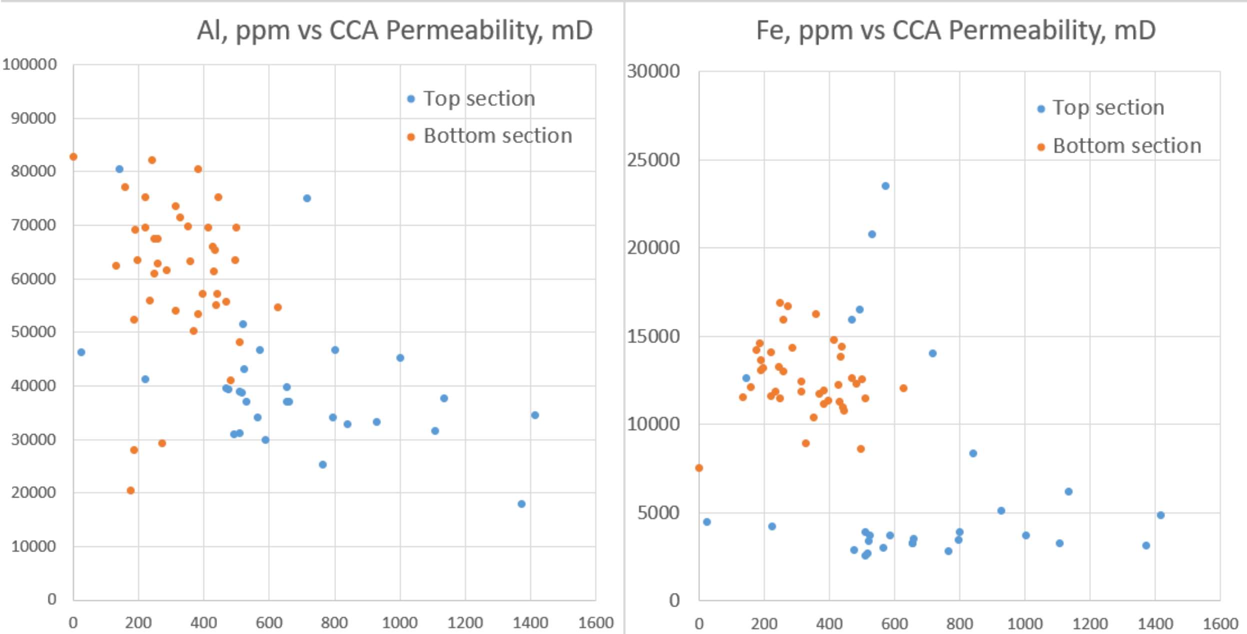

Figure 15. *Al and Fe vs CCA permeability. As it can be interpreted from the plot, the control from Fe and Al is high on permeability.*

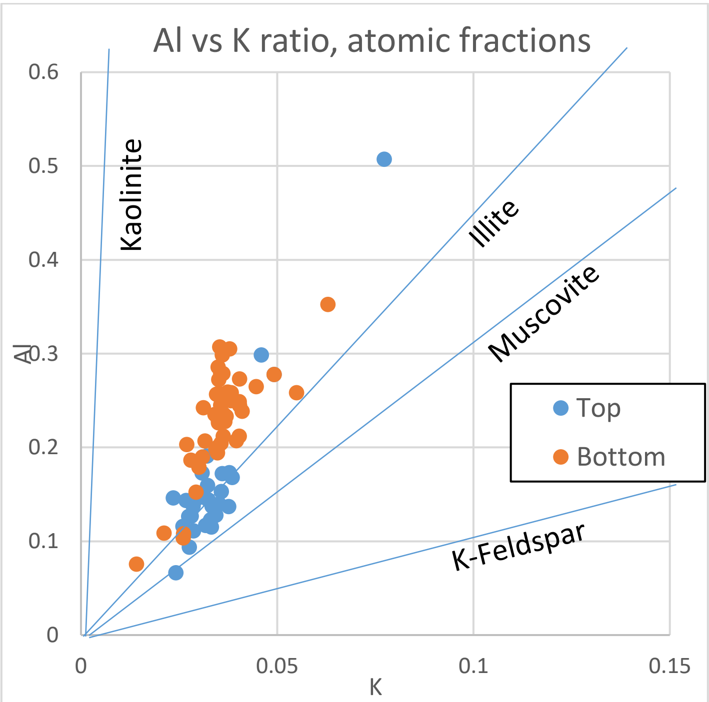

Figure 16. *The ratio between Aluminum and Potassium can differentiate clay minerals. The bottom section can have more kaolinite, while top section, having fewer clay minerals, K-Feldspar can be seen more. Uncertainty is that if you have trends showing illite and muscovite type of clay it can just show good relationship between kaolinite and K-feldspar.*

How does grain size relate to chemistry (Fe, Al, Si, Ca, Ti, etc) or Si/Si+Al?

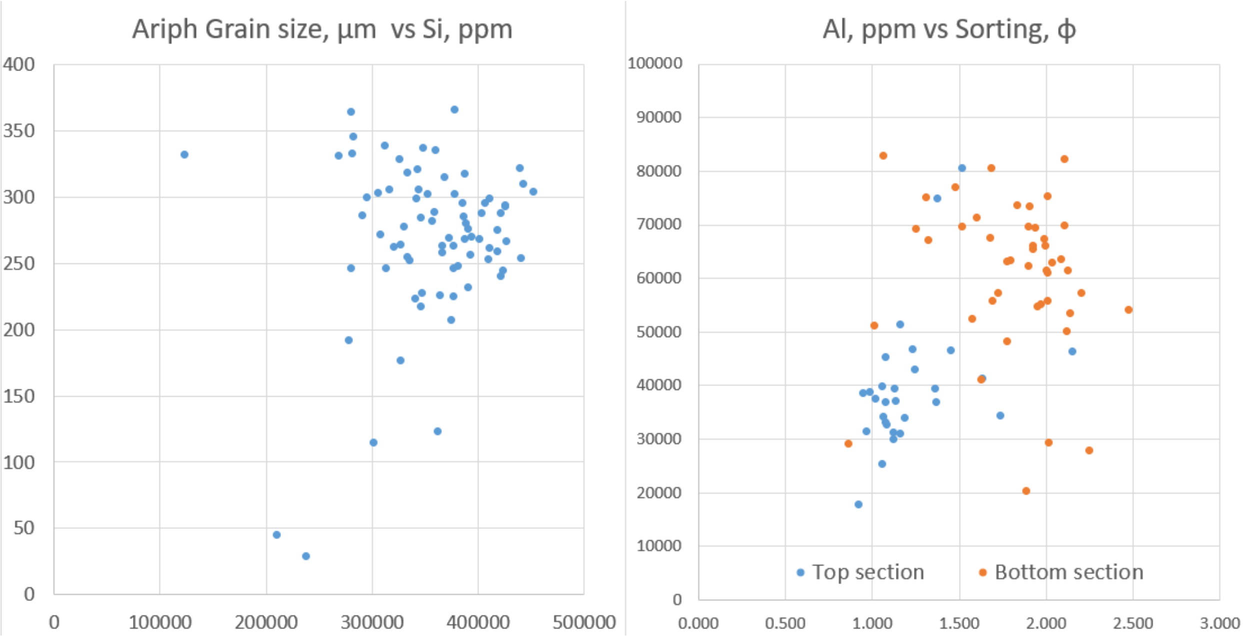

Figure 17. *On the left relationship between arithmetic grain size and Si is seen. It shows minor trend on the control on the grain size from the composition of Si. On the right relationship between Al and sorting exhibits the trend of the more Al is presenting in composition the poorer sorting it reflects.*

How do QEMSCAN, XRD and light optics relate to XRF data and CCA?

As XRD data was also derived but with limited referenced to the vertical stratigraphy (fewer samples), it can be compared to the XRF results. Results seen in table 5 can correspond to the interpretation from XRF. Light optics also confirms the interpretation from all combined methods and resulting in the same conclusion.

Results of the XRF in this work can also be used to compare it to QEMSCAN/XRD results. Presence of Si can reflect the quartz mineral; Al, Fe, K can reflect the clay minerals such as K-feldspar, kaolinite, illite and plagioclase; Ca is related to calcite cementation and carbonate minerals; S combined with Fe can give information about the presence of Pyrite etc. Due to less time involved and low price, XRF can be used to characterize the composition instead of XRD and can give data with almost the same information.

The Mey sandstone from the wireline log and even from the core description can be seen as homogeneous with minor variation in reservoir quality. However, after the all combined results, it cannot be interpreted as homogeneous reservoir. From the other hand, claiming that the reservoir has enough heterogeneity is also can lead to wrong path, considering that the Mey sandstone has relatively moderate reservoir quality within the whole stratigraphy and connection between the intervals. The main control, however, can be the claystone clasts, sorting and clay presence.

The further study of the rock can relate to the investigation spatial distribution of the reservoir. It causes uncertainty on how the Mey sandstone is variable horizontally.

In terms of the behaviour of the reservoir while CO_2 injection, sandstone generally is claimed to be a good reservoir (Bradshaw and Dance 2005). Pure quartz is inert to CO_2 since quartz does not show changes in solubility because function of pH below pH 9. However, felspar and lithic rich sandstones are potentially reactive to CO2 since they contain non-carbonate minerals and they can react to make carbonate minerals. So high Fe content found in the bottom part and related to high pyrite causes further research and investigation how it can react with the injection of CO_2. Calcite-cemented intervals are typically in equilibrium with CO2 and it can cause only a small degree of additional mineral dissolution. However, initial carbonate dissolution might be later superseded by silicate dissolution and growth of new carbonate minerals (Worden and Smith 2004). Therefore, further speculation of CO2 injection and its reaction is not the part of current discussion.

Conclusion

1. In terms of facies that are recognized for the Mey sandstone, amalgamated sandstone is dominant with the cap of the hemipelagic mudstone. It is interpreted as non-cohesive high-density turbidite sandstones and low energy hemipelagic mudstones. Sandstones have the reservoir quality and was proved as the hydrocarbon-bearing porous and permeable reservoir. Mudstones can play the role of low-permeable clasts that can affect the vertical permeability in several intervals. Another feature that should be considered is cemented intervals (one in place cemented clast and several 1ft long rounded cemented nodules) that can affect vertical permeability (cemented clast at 7221ft) and net-to-gross ratio (rounded nodules). Two core sections (core 1 and core 2) were identified and have following differences in sandstones: top section is dark-brown coloured and interbedded with claystone clasts; bottom section is olive-grey coloured, continuous and with cemented nodules.

   CCA derived porosity and permeability reflected the vertical stratigraphy. Porosity has a minor variation and slightly increasing upwards from 20% to 26-27%. Permeability has a significant variation from bottom to top sections and increasing approximately from 200mD to 1400mD. In places cemented intervals have substantial impact on porosity (4%) and permeability (0.23mD). Claystone clasts are present between the samples and might control the permeability variation in neighbouring samples on the top sections.
2. Grain size and sorting data were derived to assess the control on reservoir quality. Grain size has minor variation as the type of amalgamated sandstone consists of fine to medium sand grain size due to depositional characteristic. However, the sorting can reveal that homogeneity of the sandstone is not explicit. Better sorting (derived from Folk and Ward method) in the top section corresponds to the permeability increase upwards. As a result, sorting of the sandstone is revealed as the main control on the reservoir quality (on permeability).
3. Chemostratigraphic analysis was attempted to assess the composition of the Mey sandstone. Si is the most abundant chemical element in this reservoir rock and reflected that the quartz mineral composition is dominant for the sandstone and higher its presence corresponds to the top section. Moreover, Al, Fe and K, that are characterized by the clay elements, can explain that poorer sorting on the bottom part corresponds to more clay content within the sandstone. Fe, along with S, reveals that its high content in the bottom section of the core related to pyrite minerals. Additionally, high Ca values correspond to the cemented intervals confirming calcite nature of the cement. In summary, chemical composition reveals that clay content is a significant control and affects the sorting of the Mey sandstone, that is, in turn, affects the reservoir quality. Core as the source of data is differentiated to top and the bottom. The top section is characterized by better reservoir quality, sorting, less clay content and interbedded with the claystone clasts. Bottom section with continuous vertical stratigraphy has the poorer sorting, more clay content, calcite cemented intervals and uncommon high pyrite minerals.

References

BLOTT, S.J. & PYE, K. 2001. GRADISTAT: a grain size distribution and statistics package for the analysis of unconsolidated sediments. *Earth Surface Processes and Landforms*, **26**, 1237-1248.

BRADSHAW, J. & DANCE, T. 2005. Mapping geological storage prospectivity of CO2 for the world's sedimentary basins and regional source to sink matching. *Greenhouse Gas Control Technologies*, **7**, 583-591.

CHAWCHAI, S., KYLANDER, M.E., CHABANGBORN, A., LOWEMARK, L. & WOHLFARTH, B. 2016. Testing commonly used X-ray fluorescence core scanning-based proxies for organic-rich lake sediments and peat. Boreas, **45**, 180-189.

DAVIS, C., HAUGHTON, P., MCCAFFREY, W., SCOTT, E., HOGG, N., & KITCHING, D. 2009. Character and distribution of hybrid sediment gravity flow deposits from the outer Forties Fan, Palaeocene Central North Sea, UKCS. *Marine and Petroleum Geology*, **26(10)**, 1919–1939. doi:10.1016/j.marpetgeo.2009.02.015

DEEGAN, C. & SCULL, B.J. 1977. *A Standard Lithostratigraphic Nomenclature for the Central and Northern North Sea*. Institute of Geological Sciences Report 77/25.

ESHEL, G., LEVY, G. J., MINGELGRIN, U., & SINGER, M. J. 2004. Critical Evaluation of the Use of Laser Diffraction for Particle-Size Distribution Analysis. *Soil Science Society of America Journal*, **68**(3), 736. doi:10.2136/sssaj2004.7360

FISHER, L., GAZLEY, M.F., BAENSCH, A., BARNES, S.J., CLEVERLEY, J. & DUCLAUX, G. 2014. Resolution of geochemical and lithostratigraphic complexity: a workflow for application of portable X-ray fluorescence to mineral exploration. *Geochemistry-Exploration Environment Analysis*, **14**, 149- 159.

FLUDE, S., ALCADE, J., WILKINSON, M., JOHNSON, G., EDLMANN, K., BOND, C. & HASZELDINE, R. S. 2018, April. Quantifying geological CO2 storage security to deliver on climate mitigation. *EGU General Assembly Conference Abstracts*, **20**, 8389.

FOLK, R.L. AND WARD, W.C. 1957. Brazos River bar: a study in the significance of grain size parameters. *Journal of Sedimentary Petrology*, **27**, 3-26.

GLENNIE, K.W. ed. 2009. Petroleum Geology of the North Sea: Basic concepts and recent advances. John Wiley & Sons.

HASZELDINE, R. S., FLUDE, S., JOHNSON, G., & SCOTT, V. 2018. Negative emissions technologies and carbon capture and storage to achieve the Paris Agreement commitments. *Philosophical Transactions of the Royal Society A: Mathematical, Physical and Engineering Sciences*, **376,** 2119, 20160447.

HAUGHTON, P.D.W., BARKER, S.P., & MCCAFFREY, W.D. 2003. "Linked" debrites in sand-rich turbidite systems - origin and significance. *Sedimentology,* **50(3),** 459–482. doi:10.1046/j.1365-3091.2003.00560.x

HAUGHTON, P.D.W., DAVIS, C., & MCCAFFREY, W., 2006, Facies prediction in turbidite fan systems – nature and significance of 'linked debrites' in sand-rich versus mixed sand-mud systems recent advances in siliciclastic facies models: implications for reservoir characterization II (SEPM), *AAPG Annual Convention*, April 9-12, 2006 Technical Program

JENKINS, R. 1999. X-ray Fluorescence Spectrometry. Wiley-Interscience, New York.

KILHAMS, B., HARTLEY, A., HUUSE, M., & DAVIS, C. 2012. Characterizing the Paleocene turbidites of the North Sea: the Mey Sandstone Member, Lista Formation, UK Central Graben. *Petroleum Geoscience*, **18(3)**, 337–354. doi:10.1144/1354-079311-054

KNOX, R.W.O.B. & HOLLOWAY, S. 1992. Paleogene of the central and northern North Sea. Lithostratigraphic nomenclature of the UK North Sea. British Geological Survey, Nottingham.

KRUMBEIN, W.C. AND PETTIJOHN, F.J. 1938. Manual of Sedimentary Petrography. Appleton-Century-Crofts, New York.

LYNCH K. 2019. Accelerating CCS Technologies: Acorn Project. Research Council of Norway & Department of Business, Energy & Industrial Strategy. Pale Blue Dot Energy. http://actacorn.eu/sites/default/files/ACT%20Acorn%20Final%20Report.pdf

MAURIOHOOHO, K., BARKER, S.L.L. & RAE, A. 2016. Mapping lithology and hydrothermal alteration in geothermal systems using portable X-ray fluorescence (pXRF): A case study from the Tauhara geothermal system, Taupo Volcanic Zone. *Geothermics*, **64**, 125-134.

MILTON, N.J., BERTRAM, G.T. & VANN, I.R. 1990. Early Palaeogene tectonics and sedimentation in the Central North Sea. *In*: Hardman, R.F.P. & Brooks, J. (eds) *Tectonic Events Responsible for Britain's Oil and Gas Reserves*. Geological Society, London, Special Publications, **55**, 339‑351.

MORTON, A.C., & KNOX, R.W.O. 1990. Geochemistry of late Palaeocene and early Eocene tephras from the North Sea Basin. *Journal of the Geological Society,* **147(3)**, 425-437. https://doi:10.1144/gsjgs.147.3.0425

MUDGE, D.C. & BUJAK, J.P. 1996. An integrated stratigraphy for the Paleocene and Eocene of the North Sea. *In:* Knox, R.W., Corfield, R.M. & Dunay, R.E. (eds) *Correlation of the Early Paleogene in Northwest Europe*. Geological Society, London, Special Publications, **101**, 91‑113.

MUDGE, D.C. & COPESTAKE, P. 1992. A revised Lower Palaeogene lithostratigraphy for the Outer Moray Firth. *Marine and Petroleum Geology*, **9**, 53–69.

MULDER, T. & ALEXANDER, J., 2001. The physical character of subaqueous sedimentary density flows and their deposits. *Sedimentology*, **48(2),** 269-299.

MUTTI, E., & RICCI LUCCHI, F. 1978. Turbidites of the northern Apennines: introduction to facies analysis. *International Geology Review*, **20(2),** 125–166. doi:10.1080/00206817809471524

NORMARK, W. R. 1970. Growth patterns of deep-sea fans. *AAPG Bulletin*, **54**(11), 2170-2195.

NORMARK, W. R., & PIPER, D. J. 1972. Sediments and growth pattern of Navy deep-sea fan, San Clemente Basin, California Borderland. *The Journal of Geology*, **80**(2), 198-223.

O'CONNOR, S.J. & WALKER, D. 1993. Paleocene reservoirs of the Everest trend. *In*: Parker, J.R. (ed.) *Petroleum Geology of Northwest Europe: Proceedings of the 4th Conference*. *Geological Society*, London, 145‑160.

ROTHWELL, R.G. & RACK, F.R. 2006. New techniques in sediment core analysis: an introduction. *New Techniques in Sediment Core Analysis*, **267**, 1-29.

SHANMUGAM, G., BLOCH, R.B., MITCHELL, S.M., BEAMISH, G.W., HODGKINSON, R.J., DAMUTH, J.E., STRAUME, T., SYVERTSEN, S.E. & SHIELDS, K.E. 1995. Basin-floor fans in the North Sea: sequence stratigraphic models vs. sedimentary facies. *American Association of Petroleum Geologists Bulletin*, **79(4),** 477-511.

SHINDO, D. & OIKAWA, T. 2002. Analytical Electron Microscopy for Materials Science. SpringerVerlag, Tokyo.

STEWART, I.J., 1987. A revised stratigraphic interpretation of the Early Paleogene of the Central North Sea. *Petroleum Geology of North West Europe*. 557-576.

STOW, D.A.V. 1986. Deep clastic seas. *Sedimentary environments and facies*, 300-444.

TALLING, P.J., AMY, L.A., WYNN, R.B., PEAKALL, J., & ROBINSON, M. 2004. Beds comprising debrite sandwiched within co-genetic turbidite: origin and widespread occurrence in distal depositional environments. *Sedimentology*, **51(1),** 163–194. doi:10.1111/j.1365-3091.2004.00617.x

WALKER, R.G. 1978. Deep-water sandstone facies and ancient submarine fans: models for exploration for stratigraphic traps. *American Association of Petroleum Geologists Bulletin*, **62(6),** 932-966.

WEINDORF, D.C., ZHU, Y.D., MCDANIEL, P., VALERIO, M., LYNN, L., MICHAELSON, G., CLARK, M. & PING, C.L. 2012. Characterizing soils via portable x-ray fluorescence spectrometer: 2. Spodic and Albic horizons. Geoderma, 189, 268-277.

WORDEN, R. H., & SMITH, L. K. 2004. Geological sequestration of CO2in the subsurface: lessons from CO2injection enhanced oil recovery projects in oilfields. Geological Society, London, Special Publications, **233**(1), 211–224. doi:10.1144/gsl.sp.2004.233.01.14

WORDEN, R.H. 2019. Principles and background to the interpretation of portable XRF analytical data from sediments and sedimentary rocks. [Unpublished].

YOUNG, K.E., EVANS, C.A., HODGES, K.V., BLEACHER, J.E. & GRAFF, T.G. 2016. A review of the handheld X-ray fluorescence spectrometer as a tool for field geologic investigations on Earth and in planetary surface exploration. *Applied Geochemistry*, **72**, 77-87.

ZEP. 2015 Executable plan for enabling CCS in Europe, p. 11. See http://www. zeroemissionsplatform.eu/news/news/1650-zep-executable-plan-for-ccs-in-europe.html